Synchronization of qubits by resonator coupling

Dima Shepelyansky
www.quantware.ups-tlse.fr

Comparison of Quantum and Semiclassical Radiation Theories with Application to the Beam Maser*

E. T. JAYNES† AND F. W. CUMMINGS‡

Summary—This paper has two purposes: 1) to clarify the relationship between the quantum theory of radiation, where the electromagnetic field-expansion coefficients satisfy commutation relations, and the semiclassical theory, where the electromagnetic field is considered as a definite function of time rather than as an operator; and 2) to apply some of the results in a study of amplitude and frequency stability in a molecular beam maser.

In 1), it is shown that the semiclassical theory, when extended to take into account both the effect of the field on the molecules and the effect of the molecules on the field, reproduces almost quantitatively the same laws of energy exchange and coherence properties as the quantized field theory, even in the limit of one or a few quanta in the field mode. In particular, the semiclassical theory is shown to lead to a prediction of spontaneous emission, with the same decay rate as given by quantum electrodynamics, described by the Einstein A coefficients.

In 2), the semiclassical theory is applied to the molecular beam maser. Equilibrium amplitude and frequency of oscillation are obtained for an arbitrary velocity distribution of focused molecules, generalizing the results obtained previously by Gordon, Zeiger, and Townes for a singel-velocity beam, and by Lamb and Helmer for a Maxwellian beam. A somewhat surprising result is obtained; which is that the measurable properties of the maser, such as starting current, effective molecular Q, etc., depend mostly on the slowest 5 to 10 per cent of the molecules.

Next we calculate the effect of amplitude and frequency of oscillation, of small systematic perturbations. We obtain a prediction

* Received September 28, 1962.
† Washington University, St. Louis, Mo.
‡ Aeronutronic, Division of Ford Motor Co., Newport Beach, Calif.

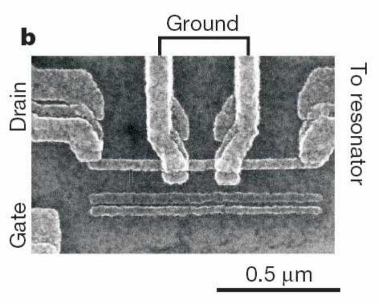

- (1963) Jaynes-Cummings model (Proc. IEEE)
- Hamiltonian:
  $\hat{H} = \hbar\omega_0\hat{n} - \hbar\Omega\sigma_x/2$
  $+g\hbar\omega_0(\hat{a}+\hat{a}^\dagger)\sigma_z + f\cos\omega t\,\left(\hat{a}+\hat{a}^\dagger\right)$
- Master equation for the density matrix:
  $\dot{\hat{\rho}} = -i[\hat{H},\hat{\rho}]/\hbar$
  $+\lambda(\hat{a}\hat{\rho}\hat{a}^\dagger - \hat{a}^\dagger\hat{a}\hat{\rho}/2 - \hat{\rho}\hat{a}^\dagger\hat{a}/2)$
- Quality factor: $Q = \omega_0/\lambda \sim 100$
  Zhirov, DS, PRL 100, 014101 (2008)
- Single artificial-atom lasing
  O. Astafiev *et al.* Nature 449, 588 (2007)

Dynamics and bistability of qubit

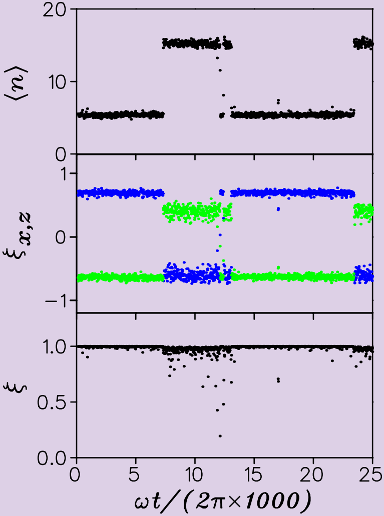

- Fig.1: Bistability of qubit coupled to a driven oscillator with jumps between two metastable states. Top panel shows average oscillator level number $\langle n \rangle$ as a function of time t at stroboscopic integer values $\omega t/2\pi$; middle panel shows the qubit polarization vector components ξ_x (blue) and ξ_z (green) at the same moments of time; the bottom panel shows the degree of qubit polarization ξ. Here the system parameters are $\lambda/\omega_0 = 0.02$, $\omega/\omega_0 = 1.01$, $\Omega/\omega_0 = 1.2$, $f = \hbar\lambda\sqrt{n_p}$, $n_p = 20$ and $g = 0.04$.

Dynamics and bistability of qubit

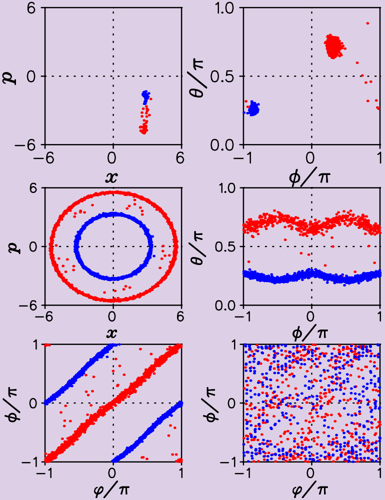

- Fig.2: Top panels: the Poincaré section taken at integer values of $\omega t/2\pi$ for oscillator with $x = \langle(\hat{a}+\hat{a}^\dagger)/\sqrt{2}\rangle$, $p = \langle(\hat{a}-\hat{a}^\dagger)/\sqrt{2}i\rangle$ (left) and for qubit polarization with polarization angles (θ, ϕ) defined in text (right). Middle panels: same quantities shown at irrational moments of $\omega t/2\pi$. Bottom panels: qubit phase ϕ *vs.* oscillator phase φ ($p/x = -\tan\varphi$) at time moments as in middle panels for $g = 0.04$ (left) and $g = 0.004$ (right). Other parameters and the time interval are as in Fig.1. The color of points is blue for $\xi_x > 0$ and red for $\xi_x < 0$.

Macroscopic detector of qubit state

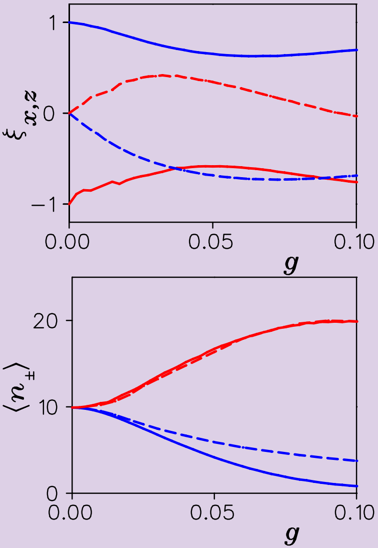

- Fig.3: Top panel: dependence of average qubit polarization components ξ_x and ξ_z (full and dashed curves) on g, averaging is done over stroboscopic times (see Fig.1) in the interval $100 \leq \omega t/2\pi \leq 2 \times 10^4$; color is fixed as in Fig.2. Bottom panel: dependence of average level of oscillator in two metastable states on coupling g, color is fixed by ξ_x sign on right panel (red for large n_+ and blue for small n_-); average is done over the quantum state and stroboscopic times as in the top panel; dashed curves show theory dependence (see text). Two QT are used with initial value $\xi_x = \pm 1$. All parameters are as in Fig.1 except g.

Macroscopic detector of qubit state

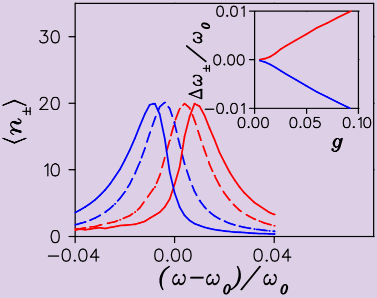

- Fig.4: Dependence of average level $n_\pm$ of oscillator in two metastable states on the driving frequency ω (average and color choice are the same as in right panel of Fig.3); coupling is $g = 0.04$ and $g = 0.08$ (dashed and full curves). Inset shows the variation of position of maximum at $\omega = \omega_\pm$ with coupling strength g, $\Delta\omega_\pm = \omega_\pm - \omega_0$. Other parameters are as in Fig.1.

Theoretical estimates: the shift $\Delta\omega_\pm$ explains two states $n_\pm$ of driven oscillator well described by $n_\pm = n_p\lambda^2/(4(\omega - \omega_0 - \Delta\omega_\pm)^2 + \lambda^2)]$ (see dashed curves in Fig.3 bottom traced with numerical values of $\Delta\omega_\pm$ from Fig.4 inset). To estimate $\Delta\omega_\pm$ we note that the frequency of effective Rabi oscillations between quasi-degenerate levels is $\Omega_R \approx g\omega_0\sqrt{n_\pm + 1}$ (JC-model) that gives $\Delta\omega_\pm \approx d\Omega_R/dn \approx \pm g\omega_0/2\sqrt{n_\pm + 1}$ in a good agreement with data.

Macroscopic quantum tunneling between qubit states

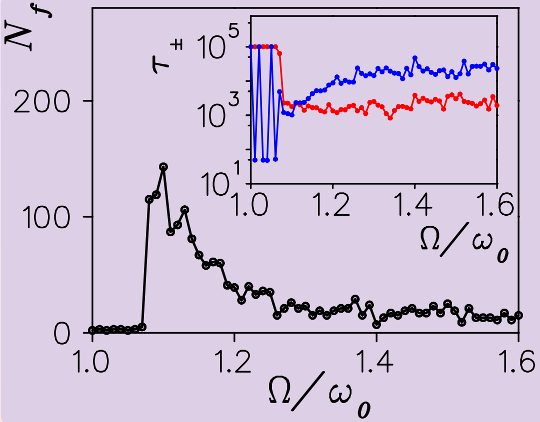

- Fig.5: Dependence of number of transitions N_f between metastable states on rescaled qubit frequency Ω/ω_0 for parameters of Fig.1; N_f are computed along 2 QT of length 10^5 driving periods. Inset shows life time dependence on Ω/ω_0 for two metastable states (τ_+ for red, τ_- for blue, $\tau_\pm$ are given in number of driving periods; color choice is as in Figs.2,3)

Radiation spectrum of qubit

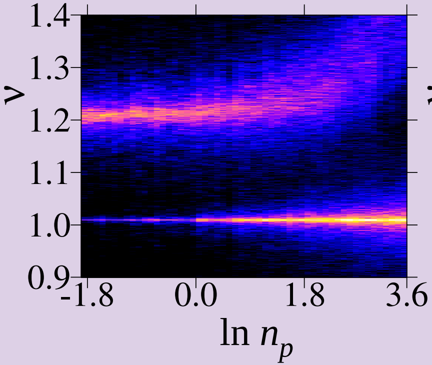

Fig.6: Spectral density $S(\nu)$ of qubit radiation $\xi_z(t)$ as function of driving power n_p in presence of phase noise in ϕ with diffusion rate $\eta = 0.004\omega_0$. Left: $\Omega/\omega_0 = 1.2$; right: $\Omega/\omega_0 = 1$. Other parameters are as in Fig.1. Color shows $S(\nu)$ in logarithmic scale (white/black for maximal/zero), ν is given in units of ω_0.

Future entanglement-enabled technologies

(part presented on blackboard)

- superconducting qubits coupled to a resonator: new sources of lasing of coherent and entangled photons
- entangled microwave photons open new prospects for microwave mobile telecom communication with complete privacy
- using coherent and entangled microwave photons for holographic imaging